ELSEVIER

Carbohydrate Polymers 51 (2003) 93–98

Carbohydrate Polymers

www.elsevier.com/locate/carbpol

Single-walled carbon nanotube—potato amylose complex

Cheng-yi Lii[a], Leszek Stobinski[b], Piotr Tomasik[c,*], Chia-ding Liao[a]

[a]*Institute of Chemistry, Academia Sinica, Nankang, 11529 Taipei, Taiwan, ROC*
[b]*Institute of Physical Chemistry, Polish Academy of Sciences, Kasprzaka Street, 44/52, 01-224 Warsaw, Poland*
[c]*Department of Chemistry, University of Agriculture, Mickiewicz Ave., 21, 31 120 Cracow, Poland*

Received 23 November 2001; revised 30 April 2002; accepted 30 April 2002

Abstract

Single-walled carbon nanotubes are wetted in aqueous solution of pure potato amylose and separated into homogenous suspension of nanotubes and sediment of bundled nanotubes. Similarly microcrystalline and colloidal graphite is wetted in the amylose solution whereas C_{60} fullerenes remained non-wetted. In the micro-Raman spectra of the amylose complexes with single-walled nanotubes, a relatively large shift of the ω_D and ω_G modes towards a higher wave number was observed. In such a spectra of complexes of microcrystalline and colloidal graphite corresponding shifts were much subtler. These changes in the spectra of nanotubes were accompanied by clear changes in the ratio of the integrated intensities of both the modes. No such changes could be noted in the spectra of amylose complexes with graphite. Optical, SEM and AFM microscopic observations of solidified complexes suggest that small nanotubes could be enveloped by amylose helices.

Keywords: Carbon nanotubes; Nano-shock spring absorber; Nanotechnology; Polysaccharides

1. Introduction

Potato amylose (PA) is a linear polymer of 1 → 4′ linked α-D-glucose units (100–200 kDa). In aqueous solution it resides in a randomly coiled chain, which becomes the host molecule of left-handed helical complex formed when a molecule with sufficiently long linear hydrophobic fragment (a guest molecule) is available. Such helical complexes with higher alkanols, lipids, and even I_5^- anion of KI_5 are well known (Tomasik & Schilling, 1998). PA in such complexes has all hydroxyl groups of its glucose units directed to the space and the channel of the helix is hydrophobic. Benefits in energy resulting from non-polar interactions between PA and the hydrophobic portion of the guest is a driving force for the complex formation. Hydrogen bonds between 3-OH group and 2-O—atom belonging to adjacent glucose units [one such bond per one turn of the helix (Stein & Rundle, 1948)] and between 2-OH group and 6-O—atom of the glucose units in adjacent turns of the helix additionally stabilise helical complex. Usually, one turn of the helix employs six glucose units. The cavity diameter of such an helix is 0.54 nm. (Immel & Lichtenthaler, 2000). When the benefit from the non-polar interactions resulting from the complex formation exceeds the energy of the intra- and inter-molecular bonds stabilising the six-membered turn the helix expands even to eight-membered turn (Yamashita, 1965; Yamashita & Hirai, 1966; Yamashita & Monobe, 1971). In such a case the cavity diameter increases to 0.97 nm corresponding to that of γ-cyclodextrin (Szejtli, 1986). Because higher-membered cyclodextrins are known, helices of amylose with over eight glucose units in one turn are likely.

Carbon nanotubes are tubular forms of elemental carbon. Single-walled carbon nanotubes (SWCNTs) have 0.4–2.5-nm diameter. The sp^2-hybridised carbon atoms on the walls have hexagonal arrangement. Therefore, the structure of nanotubes may be considered as a sheet of graphene (a single layer of graphite) folded into a tube (single-walled carbon nanotube). Nanotubes can be composed of several tubes inside of one another (multi-walled carbon nanotubes). Nanotubes are either open or closed in their ends. Caps closing nanotubes must also contain pentagons of carbon atoms is an indispensable condition to achieve closing. Surface and channel of SWCNTs are nonpolar and hydrophobic. Therefore, SWCNTs are not wetted by water and do not form aqueous suspensions. Their applications result, among others, from their unusual emissive properties

* Corresponding author. Tel./fax: +48-12-662-43-35.
E-mail address: rrtomasi@cyf-kr.edu.pl (P. Tomasik).

0144-8617/03/$ - see front matter
PII: S0144-8617(02)00122-4

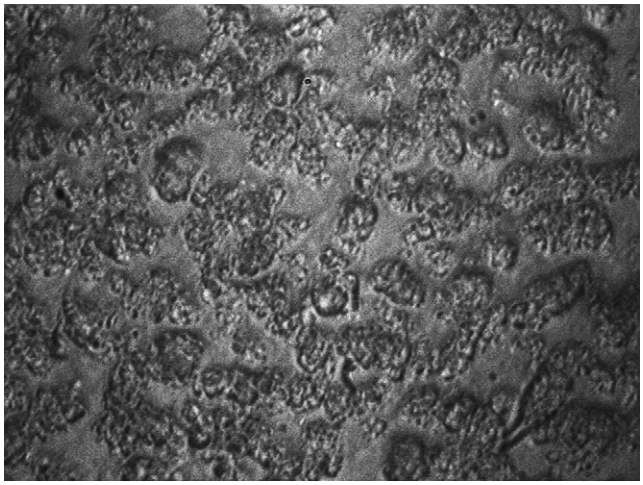

Fig. 1. Optical microscope image of a surface of thin film developed by means of evaporation of aqueous PA–SWCNT suspension on a silicon plate.

useful in electronics and an extraordinary mechanical resistance (Przygocki & Włochowicz, 2001; Saito, Dresselhaus, & Dresselhaus, 1998).

Diameter of SWCNTs suggests that the small diameter of SWCNTs might cause coiling of PA chain around them to form a nano-construction resembling a spring shock absorber. However, sorption of PA on the surface of carbon species with involvement of the lone electron pairs of the hydroxyl groups cannot be excluded. Such kind interaction should be manifested as some changes in Raman spectrum. Properties of PA and SWCNTS suggest that both the kinds of their interactions might result in the formation of PA–SWCNT complexes wetted by water. Complexation can provide isolation of SWCNTS from impurities usually accompanying them and even their segregation into fractions distinguishing from one another in size of complexed SWCNT. Finally, formation of complexes might be considered as one of several possible ways of modification of the various partners of complexes.

2. Materials and methods

Materials. Amylose was purchased from Sigma Saint Louis, MO, USA. Single-walled carbon nanotubes, SE (selected grade) of size varying between 1.2 and 1.5 nm with average size of approximately 1.3 nm were manufactured by CarboLex Inc., University of Kentucky, Lexington.

Colloidal graphite conductive adhesive 154 was purchased from Electron Microscopy Sciences, Fort, WA, USA). It was extracted and washed with acetone and methanol then centrifuged, and dried in a dry-box prior to its use. Microcrystalline graphite APS, 2–5 μm, 99.9995% was purchased from Alfa Aesar, A Johnson Matthey Co., Ward Hill, MA, USA). C_{60} fullerene (fullerite) was purchased from Aldrich Co., Milwaukee, WI, USA).

Complex formation. Aqueous solution of amylose (10 mg in 5 ml of re-distilled water) was blended with either single-walled carbon nanotubes, colloidal graphite conductive adhesive 154, microcrystalline graphite or C_{60} fullerene (~1 mg in every case). All mixtures were 30 min sonicated (Bransonic Ultrasonic Cleaner 5210R-DT, Branson Ultrasonic Corp., Danbury, CT, USA). Only fullerene did not form suspension and resided non-wetted. Resulting suspensions of SWCNTs and graphites were left to stand overnight. Greyish supernatants were thoroughly decanted from black sediment and their parts were developed on silicon support and the other parts were transferred to polyethylene conical tubes to dry them in a dry-box. Dry samples were subjected to the following tests:

Micro-Raman spectroscopy. Micro-Raman spectroscope, Renishaw Ramascope (Hewlett-Packard Co., Corvalliis Ore., USA) equipped with 514.52 nm argon laser and Olympus BH2—UMA optical microscope was used. Area of scanning was 1 μm^2. Single and triple scannings were applied. Objects of scanning were arbitrarily selected based on visible differences in the sample appearance. The precision of the measurements was estimated on $\pm 1.4\ cm^{-1}$ based on the shifts of the peak for silicon.

Optical microscopy (OM). Optical microscope with Olympus Vanox (Melville, NY, USA) AHMT 3 was applied.

Scanning electron microscopy (SEM). Scanning electron microscope with Field Emission Scanning Electron Microscope HITACHI S-4200 (Hitachi Instruments, Inc., San Jose, CA, USA) was used.

Atomic field microscopy (AFM). An atomic field microscope with Digital Instrument Vecco Metrology Group (Santa Barbara, CA, USA) Dimension TM 3100 was used. Observations were performed on gold covered samples.

Differential scanning calorimetry (DSC). Differential scanning calorimetry was performed using a Du Pont TGA System (Willmington DE, USA) scanned from 20 to 400 °C at 10°/min was performed on ~10 mg samples in 10% aqueous solutions in sealed pans.

3. Results and discussion

After blending aqueous solution of PA with SWCNTs the latter readily form suspension followed by precipitation of larger bundles in the bottom of the container. Finer parts of nanotubes resided in solution. Wetting of nanotubes in solution of surfactants is known (Ebbesen, 1996) and PA could act in such a case as surfactant. Colloidal and crystalline graphite (CGR and GR, respectively) behaved similarly on introducing them into aqueous PA whereas fullerene C_{60} remained non-wetted. Fullerenes are wetted by aqueous solution of surfactant commercially used for formation of SWCNTs suspension (for instance, single-walled carbon nanotubes (suspension of surfactance), chemically purified suspension, Grade CP, Product of

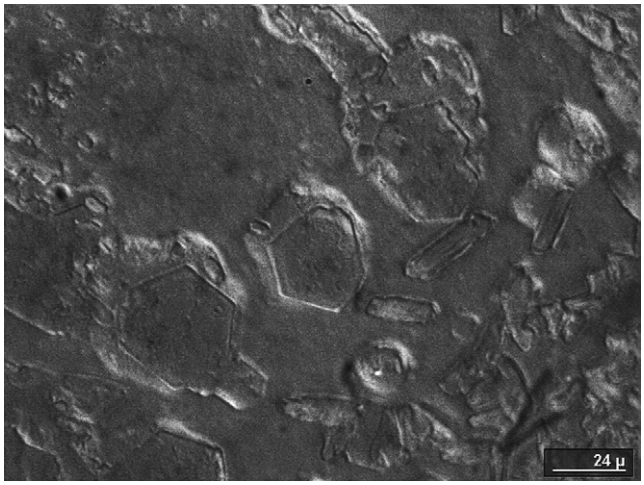

Fig. 2. Optical microscope image of thin film developed by means of evaporation of aqueous PA–SWCNT suspension. Crystalline hexagonal structures of PA can be seen apart from thin bars of PA–SWCNT complex.

CarboLex Lexington, KY). Differences in affinity of these four forms of elemental carbon, this is CGR, GR, fullerene C_{60}, and SWCNTs to PA strongly suggest that PA–GR (CGR) and PA–SWCNTs interactions might be specific and required multi-point interaction between surface of carbon species and PA. Spherical structure and size of fullerene did not provide such possibility.

Inspection of Figs. 1 and 2, which are optical micrographs of air-dried SWCNTs—aqueous PA suspension, showed SWCNTs irregularly covered with a film of PA. Dried material formed fibrils. Simultaneously, there were also large hexagonal crystals, which could be recognised as PA. It is known that PA in aqueous solutions develop its crystals of hexagonal unit cells with $a_a = 1.297$, $c_o = 0.771$, and $d_{100} = 1.123$ nm Phillips & Williams, 1961).

One might see that SWCNTs did not initiate crystallisation of PA by nucleation. An AFM micrograph (Fig. 3) of the air-dried SWCNTs suspension in aqueous PA revealed that bars could be ascribed to the structures of PA helices with SWCNTs guest inside rather than crystalline PA because none of the crystallites has an hexagonal structure and all of them have a bar shape. The surfaces of cuts of the bars are close to a square.

SEM micrographs confirmed findings from the former AFM observation.

There can be also seen thin bars apart from relatively large hexagonal structures. The bars could be assigned to SWCNTs enveloped with amylose.

The assumption that PA could form a helical inclusion complex with SWCNTs found its support in results of Raman spectra. Table 1 presents results of this investigation.

Solid, commercial PA showed two modes in the ranges of 943.6–956.3 and 2908–2915 cm^{-1}, respectively. The first band was, in fact, a doublet assigned (Phillips, Corke, Jie, Liu, & Chong, 1998) to glucose unit C–C stretching modes. The band at 1657 cm^{-1} found by Phillips et al. (1998), Phillips, Jie, Chong, Liu, and Corke (1999a) and Phillips, Jie, Liu, Pan, and Corke (1999b) in the Raman spectrum of amylose remained invisible in our spectra. After dissolving PA in water followed by evaporation to a dry PA film the low wavelength band turned into a broad band located between 967.3 and 983.0 cm^{-1}. These bands appeared in a vast majority of the spectra of GR, CGR, and SWCNTs complexes with PA and, as a rule, they were shifted to a lower wavenumber. Because the 2908–2915 cm^{-1} band in PA spectrum overlapped with the band reflecting $\omega_D + \omega_G$ modes in the spectra of SWCNTs it had a little diagnostic significance.

Complexation of every carbon species to PA produced always anti-Stokes–Raman scattering with summation of molecular vibrational transition frequency (MVTF) and original energy of scattering photon. The MVTF term and its contribution to the ω_D and ω_G modes were different for each carbon species. For GR–PA complexes this contribution was 0 and 1.4–3.2 cm^{-1} for both SWCNTs bands, respectively. Corresponding increase in the MVTF term due to complexation of PA to CGR was 5.6–5.8 and 1.4–3.2 cm^{-1} for the two bands, respectively.

Thus, complexation of PA to CGR facilitated E_{2g1} in-plane vibrations and had no influence on E_{2g2} in-plane twisting vibrations. Complexation of PA to SWCNTs produced essential increase in the MVTF term. Magnitude of this effect ranged from 7.0 to 15.6 and from 8.5 to 13.7 cm^{-1} for ω_D and ω_G vibrations, respectively. This shift of vibrational modes reflected changes in vibration symmetry from E_{1g} (1585 cm^{-1}) and A_{1g} (1587 cm^{-1}) into E_{2g} (1591 cm^{-1}) (Saito et al., 1988). Such differences could be rationalised in terms of the mode of complexation. PA could sorb on planes of GR and CGR and could not coil. Coiling around individual SWCNTs seemed to be acceptable provided formation of helix turns composed of 9, 10 and more glucose units. In every case the helical PA envelope accepted electron density from SWCNTs increasing their demands for energy required for vibrational transitions. Simultaneously, such energy benefit could be a driving force for PA to coil around SWCNTs. Lack of any changes in Raman spectrum related to the peaks of PA allowed ruling out sorption of PA on carbon species with involvement of PA hydroxyl groups.

Undoubtedly, sonication of bundles of SWCNTs could crack them into shorter and smaller species. Complexation to PA could provide opportunity for isolation of individual SWCNTs of certain length from non-disintegrated bundles. Moreover, indicated differences in the interaction of GR, GRC, and SWCNTs with PA could be considered as a facile method of purification of SWCNTs from graphite contamination. In order to prove this assumption the peaks belonging to ω_D, and ω_G modes were integrated and the I_{iD}/I_{iG} ratio was calculated. This assumption would be proved if this ratio would be affected by complexation and, simultaneously, relationship (1) would provide a result close

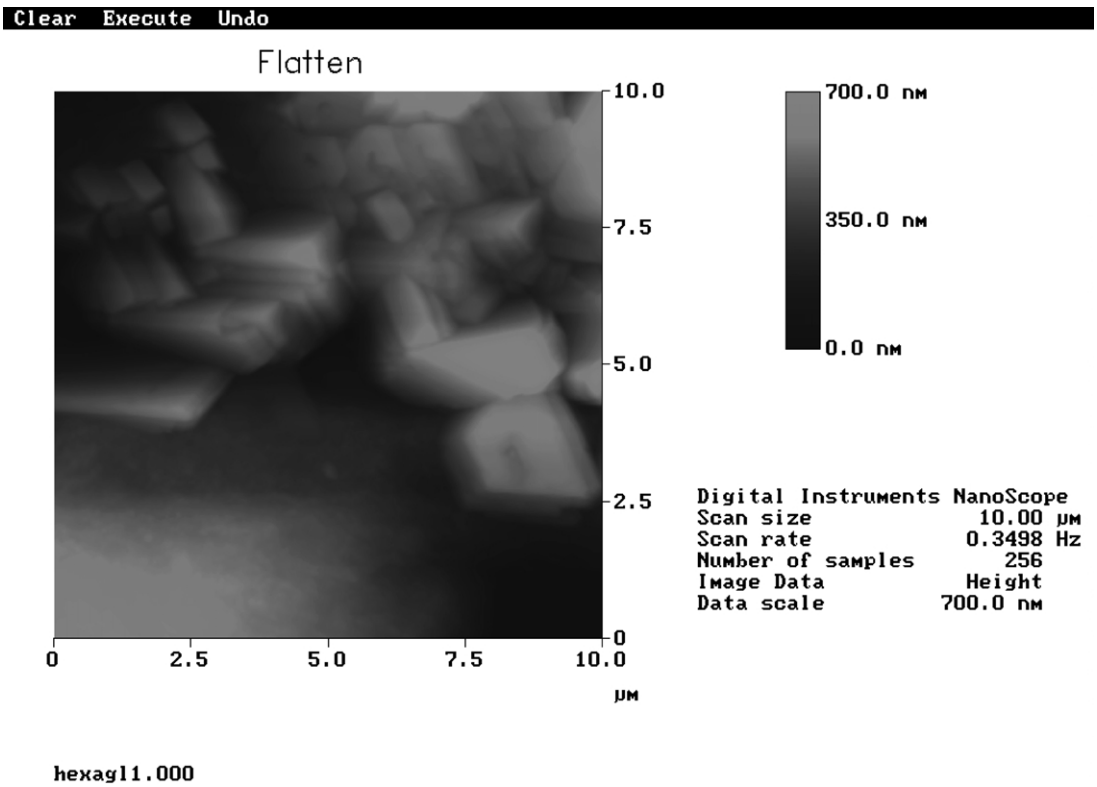

Fig. 3. AFM image of the PA–SWCNT complex.

for all complexes.

$$I_{i,1360}/I_{i,1580} = 44/L_a \quad (1)$$

where L_a is a measure of the in-plane SWCNTs crystallite size in A, is valid for the range of integrated intensities from 0.03 to 1 and for laser wavelength between 488.0 and 515.4 nm (Knight & White, 1989).

In the spectra of GR this ratio was between 0.05 and 0.04. After blending with the PA solution the 1360 cm^{-1} vibration ceased and the ratio could not be calculated. In the spectra of CGR the intensity ratio varied between 0.31 and 0.38 but its value widely scattered between 0.13 and 0.59 in the spectra of CGR–PA blends. Because the spectra were taken from various regions of the film of the complex developed on silicon surface one might suppose that complexation of CGR to PA resulted in a fractionation of the carbon species according the particle size. The magnitude of the integrated intensity ratio in the spectra of SWCNT forming suspension in the PA solution varied from 0.02 to 0.05. Eq. (1) provides L_a varying between 88 and 220 nm. Eq. (1) also showed that the in-plane crystallite size of sonicated nanotubes in the sediment varied between 88 and 49 nm as the integrated intensity ratio varied from 0.05 and 0.09. Thus, it seemed to be likely that SWCNTs might be fractionated in PA solution.

The Raman spectral pattern of the ~1590 cm^{-1} band closely resembled those published, among others, by Jorio et al. (2001). Thus, this band is preceded by another weaker band, around 1540 cm^{-1}. The ratio of the intensities of the long- and short-wavelength bands in this doublet, respectively, in the spectra of SWCNTs varied between 2.22 and 2.36. We recorded several spectra in which this ratio was between 1.71 and 2.11. However, we recorded also some spectra in which this ratio was between 2.22 and 2.55. This effect remains poorly understood. Formation of PA complexes with carbon species under study could be additionally proved by differential scanning calorimetric (DSC) measurements. PA showed only single thermal effect with onset (T_o) and peak (T_p) temperatures, respectively. Carbon species—PA complexes showed two thermal effects. The onset temperatures ranged from 68 to 72 °C for the first effects and the peak temperatures in the second effects were between 80 and 82 °C. Corresponding peak temperatures were 72–76 and 86–87 °C for the first and second effect, respectively. Enthalpies of both effects for all carbon species—PA complexes were around 2 J/g in every case. These data showed formation of carbon species with PA.

4. Conclusion

Short single-walled carbon nanotubes form complexes with amylose. The complex is formed by amylose helically enveloped around single-walled carbon nanotube. Such complex could be considered as a nano-shock-absorber. Observed behaviour of SWCNTs with respect to amylose could be considered as a method of fractionation and purification of SWCNTs.

Table 1
Positions of selected modes (ν) and the ratio of integral intensities ($I_{i,1360}/I_{i,1580}$) in Raman spectra of potato amylose (PA), diamond (DIA), graphite (GR), colloidal graphite (CGR), single-wall nanotubes (SWCNT) as well as PA–GR, PA–CGR, and PA–SWCNT complexes

Species	ω_D, ν (cm^{-1})	ω_G, ν (cm^{-1})	$I_{i,\omega_D}/I_{i,\omega_G}$	$2\omega_D$, ν (cm^{-1})	PA-bands, ν (cm^{-1})	
PA						
1					956.3[a]	2907.7
2					945.7[a]	2911.9
3					943.6[a]	2914.7
4					967.3[b]	2909.1
5					971.8[b]	2914.7
6					983.0[b]	2914.7
7					976.0[b]	2914.7
DIA						
1	1334.3					
GR						
1	1356.4	1579.6	0.05	2723.2		
2	1352.2	1579.6	0.04	2723.2		
PA–GR[c]						
1a	1356.4	1583.8	?	2729.4	943.7	
1b	1356.4	1582.4	?	2729.4	945.1	
2a	1352.3	1582.4	?	2729.4	945.1	
2b	1356.0	1582.4	?	2729.4	956.3	
3a	1356.2	1581.0	?	2729.4	966.1	
3b	1356.4	1582.4	?	2728.0	954.9	
CGR						
1	1352.3	1582.5	0.38	2723.0		
2	1352.3	1581.1	0.37	2722.5		
3	1352.3	1576.9	0.34	2722.5		
4	1353.7	1576.9	0.31	2722.5		
5	1353.7	1576.9	0.35	2721.0		
6	1352.3	1576.9	0.34	2721.1		
PA–CGR[c]						
1a	1357.1	1583.9	0.59	2729.5	977.4	
1b	1357.9	1582.5	0.13	2726.7	956.4	
2a	1359.3	1581.1	0.32	2726.7	973.2	
2b	1358.0	1581.1	0.46	2726.7	966.2	
SWCNT						
1	1335.4	1583.8	0.62	2663.4		
2	1335.4	1585.2	0.56	2663.6		
3	1335.4	1585.2	0.72	2663.4		
4	1335.4	1585.2	0.71	2663.4		
5	1335.4	1585.2	0.15	2663.4		
6	1335.4	1583.8	0.03	2663.4		
PA–SWCNT[c,d]						
1a	1346.6	1595.1	>0.01	2684.5	977.3	
1b	1346.6	1595.1	>0.01	2684.5	977.3	
2b	1346.6	1596.5	>0.01	2684.5	977.3	
3b	1346.0	1596.5	>0.01	2684.5	969.0	
4a	1342.4	1593.7	>0.01	2684.5	974.6	
4b	1346.6	1592.3	>0.01	2685.9	977.4	
5a	1346.6	1592.3	0.08	2685.9	977.4	
5b	1346.6	1595.1	0.08	2684.5	977.4	
6b	1342.4	1593.7	0.07	2684.5	959.1	
7a	1343.8	1593.7	0.09	2681.7	957.7	
7b	1349.0	1593.9	0.04	2684.1	964.1	
8a	1346.2	1596.7	0.05	2684.1	973.9	
8b	1349.0	1595.3	0.07	2686.9	952.9	
9a	1346.2	1596.7	0.04	2684.1	961.3	
9b	1343.9	1593.9	0.05	2682.7	966.9	

(*continued on next page*)

Table 1 (*continued*)

Species	ω_D, ν (cm^{-1})	ω_G, ν (cm^{-1})	$I_{i,\omega_D}/I_{i,\omega_G}$	$2\omega_D$, ν (cm^{-1})	PA-bands, ν (cm^{-1})
10a	1346.2	1593.9	0.04	2684.1	976.7
10b	1344.8	1595.3	0.04	2684.1	971.1
11a	1346.2	1595.3	0.06	2684.1	973.9
11b	1347.6	1596.7	0.03	2682.7	966.9
12a	1346.2	1592.5	>0.01	2679.9	976.7
13a	1347.0	1596.7	0.04	2685.5	954.3
13b	1346.6	1596.3	0.05	2686.9	954.3
14a	1344.8	1593.9	0.02	2684.1	979.5
14b	1346.2	1596.7	>0.01	2686.9	966.9
15a	1344.8	1595.3	0.04	2686.9	966.9
15b	1346.2	1596.7	>0.01	2686.9	955.7
16a	1346.2	1596.7	0.05	2686.9	975.3
16b	1346.2	1595.3	0.04	2685.5	965.5
17a	1347.6	1596.7	0.05	2686.9	944.5
17b	1346.1	1595.3	0.04	2684.1	941.7
18a	1343.4	1592.5	0.05	2686.9	957.1
18b	1343.6	1595.3	0.04	2684.1	968.3

[a] The commercial solid sample.
[b] Sample recovered from aqueous solution after evaporation.
[c] Samples are usually grouped in pairs. Samples denoted by 'a' were single-scanned, and samples denoted by 'b' were scanned three times.
[d] Samples 1–4 and 9–18 were those from suspension, whereas samples 5–8 were those which sedimented on the bottom. Samples 1–4, and 9, 10 were sonicated for 5 and 30 min, respectively. Samples 11–13, and 14–17 were sonicated for 60, and 90 min, respectively. Sample 18 was a combination of samples sonicated for 30–90 min.

References

Ebbesen, T. W. (1996). Wetting, filling, and decorating carbon nanotubes. *Journal of Physical Chemistry of Solids*, *57*, 951–955.

Immel, S., & Lichtenthaler, F. W. (2000). The hydrophobic topographies of amylose and its blue iodine complex. *Starch/Staerke*, *52*, 1–8.

Jorio, P., Brown, S. D. M., Marucci, A., Pimenta, M. A., Kneipp, K., Dresselhaus, G., & Dresselhaus, M. S. (2001). Surface-enhanced resonant Raman spectroscopy of single-wall carbon nanotubes adsorbed on silver and gold surfaces. *Physical Review*, *B61*, 13202–13211.

Knight, D. S., & White, W. B. (1989). Characterization of diamond films by Raman spectroscopy. *Journal of Material Research*, *4*, 385–393.

Phillips, D. L., Corke, H., Jie, X., Liu, H., & Chong, C. K. (1998). Raman spectroscopic determination of the percent of acetylation in modified starch. *Analytical Letters*, *31*, 2105–2114.

Phillips, D. L., Jie, X., Chong, C. K., Liu, H., & Corke, H. (1999a). General application of Raman spectroscopy for determination of level of acetylation of modified starches. *Cereal Chemistry*, *76*, 429–443.

Phillips, D. L., Jie, X., Liu, H., Pan, D.-H., & Corke, H. (1999b). Potential use of Raman spectroscopy for determination of amylose content in maize starch. *Cereal Chemistry*, *76*, 821–823.

Phillips, A. T., & Williams, V. R. (1961). An investigation of varietal differences in the iodine-binding capacities of crystalline rice amylose. *Journal of Food Science*, *26*, 573–577.

Przygocki, W., & Włochowicz, A. (2001). *Fullerenes and nanotubes (in Polish)*. Warsaw: WNT, Chapter 12.

Saito, R., Dresselhaus, G., & Dresselhaus, M. S. (1998). *Physical properties of carbon nanotubes*. London: Imperial College Press, p. 198.

Stein, R. S., & Rundle, R. E. (1948). On nature of the interaction between starch and iodine. *Journal of Chemical Physics*, *16*, 195–207.

Szejtli, J. (1986). *Cyclodextrin inclusion complexes*. Budapest: Akademiai Kiado.

Tomasik, P., & Schilling, C. H. (1998). Complexes of starch with inorganic guests. *Advances in Carbohydrate Chemistry and Biochemistry*, *53*, 263–344.

Yamashita, Y. (1965). Single crystals of amylose V complexes (I). *Journal of Polymer Sciences, Part A*, *3*, 3251–3260.

Yamashita, Y., & Hirai, N. (1966). Single crystals of amylose V complexes (II). Crystals with 7_1 helical configuration. *Journal of Polymer Sciences, Part A-2*, *2*, 161–171.

Yamashita, Y., & Monobe, K. (1971). Single crystals of amylose V complexes. Crystals with 8_1 helical configuration. *Journal of Polymer Sciences, Part A-2*, *9*, 1471–1478.